

# Analysis of high-performance tensor-matrix multiplication with BLAS

Cem Savaş Başsoy<sup>a,\*</sup>

<sup>a</sup>*Hamburg University of Technology, Schwarzenbergstrasse 95, 21071, Hamburg, Germany*

---

## Abstract

The tensor-matrix multiplication is a basic tensor operation required by various tensor methods such as the ALS and the HOSVD. This paper presents flexible high-performance algorithms that compute the tensor-matrix product according to the Loops-over-GEMM (LoG) approach. Our algorithms can process dense tensors with any linear tensor layout, arbitrary tensor order and dimensions all of which can be runtime variable. We discuss different tensor slicing methods with parallelization strategies and propose six algorithm versions that call BLAS with subtensors or tensor slices. Their performance is quantified on a set of tensors with various shapes and tensor orders. Our best performing version attains a median performance of 1.37 double precision Tflops on an Intel Xeon Gold 6248R processor using Intel's MKL. We show that the tensor layout does not affect the performance significantly. Our fastest implementation is on average at least 14.05% and up to 3.79x faster than other state-of-the-art approaches and actively developed libraries like Libtorch and Eigen.

---

## 1. Introduction

Tensor computations are found in many scientific fields such as computational neuroscience, pattern recognition, signal processing and data mining [1, 2]. These computations use basic tensor operations as building blocks for decomposing and analyzing multidimensional data which are represented by tensors [3, 4]. Tensor contractions are an important subset of basic operations that need to be fast for efficiently solving tensor methods.

There are three main approaches for implementing tensor contractions. The Transpose Transpose GEMM Transpose (TTGT) approach reorganizes tensors in order to perform a tensor contraction using optimized implementations of the general matrix multiplication (GEMM) [5, 6]. GEMM-like Tensor-Tensor multiplication (GETT) method implement macro-kernels that are similar to the ones used in fast GEMM implementations [7, 8]. The third method is the Loops-over-GEMM (LoG) or the BLAS-based approach in which Basic Linear Algebra Subprograms (BLAS) are utilized with multiple tensor slices or subtensors if possible [9, 10, 11, 12]. The BLAS are considered the de facto standard for writing efficient and portable linear algebra software, which is why nearly all processor vendors provide highly optimized BLAS implementations. Implementations of the LoG and TTGT approaches are in general easier to maintain and faster to port than GETT implementations which might need to adapt vector instructions or blocking parameters according to a processor's microarchitecture.

In this work, we present high-performance algorithms for the tensor-matrix multiplication which is used in many numerical methods such as the alternating least squares method [3, 4]. It is a compute-bound tensor operation and has the same arithmetic intensity as a matrix-matrix multiplication which can almost reach the practical peak performance of a computing machine.

To our best knowledge, we are the first to combine the LoG approach described in [12, 13] for tensor-vector multiplications with the findings on tensor slicing for the tensor-matrix multiplication in [10]. Our algorithms support dense tensors with any order, dimensions and any linear tensor layout including the first- and the last-order storage formats for any contraction mode all of which can be runtime variable. They compute the tensor-matrix product in parallel using efficient GEMM without transposing or flattening tensors. Despite their high performance, all algorithms are layout-oblivious and provide a sustained performance independent of the tensor layout and without tuning.

Moreover, every proposed algorithm can be implemented with less than 150 lines of c++ code where the algorithmic complexity is reduced by the BLAS implementation and the corresponding selection of subtensors or tensor slices. We have provided an open-source c++ implementation of all algorithms and a python interface for convenience. While Intel's MKL is used for our benchmarks, the user is free to select any other library that provides the BLAS interface and even integrate it's own implementation to be library independent.

The analysis in this work quantifies the impact of the tensor layout, the tensor slicing method and parallel execution of slice-matrix multiplications with varying con-

---

\*Corresponding author

Email address: [cem.bassoy@gmail.com](mailto:cem.bassoy@gmail.com) (Cem Savaş Başsoy)

traction modes. The runtime measurements of our implementations are compared with state-of-the-art approaches discussed in [7, 8, 14] including Libtorch and Eigen. In summary, the main findings of our work are:

- A tensor-matrix multiplication can be implemented by an in-place algorithm with 1 GEMV and 7 GEMM calls, supporting all combinations of contraction mode, tensor order and dimensions for any linear tensor layout.
- Our fastest algorithm with tensor slices is on average 17% faster than Intel’s batched GEMM implementation when the contraction and leading dimensions of the tensors are greater than 256.
- The proposed algorithms are layout-oblivious. Their performance does not vary significantly for different tensor layouts if the contraction conditions remain the same.
- Our fastest algorithm computes the tensor-matrix multiplication on average, by at least 14.05% and up to a factor of 3.79 faster than other state-of-the-art library implementations, including LibTorch and Eigen.

The remainder of the paper is organized as follows. Section 2 presents related work. Section 3 introduces some notation on tensors and defines the tensor-matrix multiplication. Algorithm design and methods for slicing and parallel execution are discussed in Section 4. Section 5 describes the test setup. Benchmark results are presented in Section 6. Conclusions are drawn in Section 7.

## 2. Related Work

Springer et al. [7] present a tensor-contraction generator TCCG and the GETT approach for dense tensor contractions that is inspired from the design of a high-performance GEMM. Their unified code generator selects implementations from generated GETT, LoG and TTGT candidates. Their findings show that among 48 different contractions 15% of LoG-based implementations are the fastest.

Matthews [8] presents a runtime flexible tensor contraction library that uses GETT approach as well. He describes block-scatter-matrix algorithm which uses a special layout for the tensor contraction. The proposed algorithm yields results that feature a similar runtime behavior to those presented in [7].

Li et al. [10] introduce InTensLi, a framework that generates in-place tensor-matrix multiplication according to the LOG approach. The authors discuss optimization and tuning techniques for slicing and parallelizing the operation. With optimized tuning parameters, they report a speedup of up to 4x over the TTGT-based MATLAB tensor toolbox library discussed in [5].

Başsoy [12] presents LoG-based algorithms that compute the tensor-vector product. They support dense tensors with linear tensor layouts, arbitrary dimensions and tensor order. The presented approach is to divide into eight TTV cases calling GEMV and DOT. He reports average speedups of 6.1x and 4.0x compared to implementations that use the TTGT and GETT approach, respectively.

Pawlowski et al. [13] propose morton-ordered blocked layout for a mode-oblivious performance of the tensor-vector multiplication. Their algorithm iterates over blocked tensors and perform tensor-vector multiplications on blocked tensors. They are able to achieve high performance and mode-oblivious computations.

## 3. Background

### 3.1. Tensor Notation

An order- $p$  tensor is a  $p$ -dimensional array where tensor elements are contiguously stored in memory [15, 3]. We write  $a$ ,  $\mathbf{a}$ ,  $\mathbf{A}$  and  $\underline{\mathbf{A}}$  in order to denote scalars, vectors, matrices and tensors. If not otherwise mentioned, we assume  $\underline{\mathbf{A}}$  to have order  $p > 2$ . The  $p$ -tuple  $\mathbf{n} = (n_1, n_2, \dots, n_p)$  will be referred to as the shape or dimension tuple of a tensor where  $n_r > 1$ . We will use round brackets  $\underline{\mathbf{A}}(i_1, i_2, \dots, i_p)$  or  $\underline{\mathbf{A}}(\mathbf{i})$  to denote a tensor element where  $\mathbf{i} = (i_1, i_2, \dots, i_p)$  is a multi-index. For convenience, we will also use square brackets to concatenate index tuples such that  $[\mathbf{i}, \mathbf{j}] = (i_1, i_2, \dots, i_r, j_1, j_2, \dots, j_q)$  where  $\mathbf{i}$  and  $\mathbf{j}$  are multi-indices of length  $r$  and  $q$ , respectively.

### 3.2. Tensor-Matrix Multiplication

Let  $\underline{\mathbf{A}}$  and  $\underline{\mathbf{C}}$  be order- $p$  tensors with shapes  $\mathbf{n}_a = ([\mathbf{n}_1, n_q, \mathbf{n}_2])$  and  $\mathbf{n}_c = ([\mathbf{n}_1, m, \mathbf{n}_2])$  where  $\mathbf{n}_1 = (n_1, n_2, \dots, n_{q-1})$  and  $\mathbf{n}_2 = (n_{q+1}, n_{q+2}, \dots, n_p)$ . Let  $\mathbf{B}$  be a matrix of shape  $\mathbf{n}_b = (m, n_q)$ . A  $q$ -mode tensor-matrix product is denoted by  $\underline{\mathbf{C}} = \underline{\mathbf{A}} \times_q \mathbf{B}$ . An element of  $\underline{\mathbf{C}}$  is defined by

$$\underline{\mathbf{C}}([\mathbf{i}_1, j, \mathbf{i}_2]) = \sum_{i_q=1}^{n_q} \underline{\mathbf{A}}([\mathbf{i}_1, i_q, \mathbf{i}_2]) \cdot \mathbf{B}(j, i_q) \quad (1)$$

with  $\mathbf{i}_1 = (i_1, \dots, i_{q-1})$ ,  $\mathbf{i}_2 = (i_{q+1}, \dots, i_p)$  where  $1 \leq i_r \leq n_r$  and  $1 \leq j \leq m$  [10, 4]. Mode  $q$  is called the contraction mode with  $1 \leq q \leq p$ . The tensor-matrix multiplication generalizes the computational aspect of the two-dimensional case  $\mathbf{C} = \mathbf{B} \cdot \mathbf{A}$  if  $p = 2$  and  $q = 1$ . Its arithmetic intensity is equal to that of a matrix-matrix multiplication and is not memory-bound.

In the following, we assume that the tensors  $\underline{\mathbf{A}}$  and  $\underline{\mathbf{C}}$  have the same tensor layout  $\pi$ . Elements of matrix  $\mathbf{B}$  can be stored either in the column-major or row-major format. The tensor-matrix multiplication with  $i_q$  iterating over the second mode of  $\mathbf{B}$  is also referred to as the  $q$ -mode product which is a building block for tensor methods

such as the higher-order orthogonal iteration or the higher-order singular value decomposition [4]. Please note that the following method can be applied, if indices  $j$  and  $i_q$  of matrix  $\mathbf{B}$  are swapped.

### 3.3. Subtensors

A subtensor references elements of a tensor  $\mathbf{A}$  and is denoted by  $\mathbf{A}'$ . It is specified by a selection grid that consists of  $p$  index ranges. In this work, an index range of a given mode  $r$  shall either contain all indices of the mode  $r$  or a single index  $i_r$  of that mode where  $1 \leq r \leq p$ . Subtensor dimensions  $n'_r$  are either  $n_r$  if the full index range or 1 if a single index for mode  $r$  is used. Subtensors are annotated by their non-unit modes such as  $\mathbf{A}'_{u,v,w}$  where  $n_u > 1$ ,  $n_v > 1$  and  $n_w > 1$  for  $1 \leq u \neq v \neq w \leq p$ . The remaining single indices of a selection grid can be inferred by the loop induction variables of an algorithm. The number of non-unit modes determine the order  $p'$  of subtensor where  $1 \leq p' < p$ . In the above example, the subtensor  $\mathbf{A}'_{u,v,w}$  has three non-unit modes and is thus of order 3. For convenience, we might also use an dimension tuple  $\mathbf{m}$  of length  $p'$  with  $\mathbf{m} = (m_1, m_2, \dots, m_{p'})$  to specify a mode- $p'$  subtensor  $\mathbf{A}'_{\mathbf{m}}$ . An order-2 subtensor of  $\mathbf{A}'$  is a tensor slice  $\mathbf{A}'_{u,v}$  and an order-1 subtensor of  $\mathbf{A}'$  is a fiber  $\mathbf{a}'_u$ .

### 3.4. Linear Tensor Layouts

We use a layout tuple  $\boldsymbol{\pi} \in \mathbb{N}^p$  to encode all linear tensor layouts including the first-order or last-order layout. They contain permuted tensor modes whose priority is given by their index. For instance, the general  $k$ -order tensor layout for an order- $p$  tensor is given by the layout tuple  $\boldsymbol{\pi}$  with  $\pi_r = k - r + 1$  for  $1 < r \leq k$  and  $r$  for  $k < r \leq p$ . The first- and last-order storage formats are given by  $\boldsymbol{\pi}_F = (1, 2, \dots, p)$  and  $\boldsymbol{\pi}_L = (p, p-1, \dots, 1)$ . An inverse layout tuple  $\boldsymbol{\pi}^{-1}$  is defined by  $\boldsymbol{\pi}^{-1}(\boldsymbol{\pi}(k)) = k$ . Given a layout tuple  $\boldsymbol{\pi}$  with  $p$  modes, the  $\pi_r$ -th element of a stride tuple is given by  $w_{\pi_r} = \prod_{k=1}^{r-1} n_{\pi_k}$  for  $1 < r \leq p$  and  $w_{\pi_1} = 1$ . Tensor elements of the  $\pi_1$ -th mode are contiguously stored in memory. The location of tensor elements is determined by the tensor layout and the layout function. For a given tensor layout and stride tuple, a layout function  $\lambda_{\mathbf{w}}$  maps a multi-index to a scalar index with  $\lambda_{\mathbf{w}}(\mathbf{i}) = \sum_{r=1}^p w_r(i_r - 1)$ , see [16, 13].

### 3.5. Flattening and Reshaping

The following two operations define non-modifying reformatting transformations of dense tensors with contiguously stored elements and linear tensor layouts.

The flattening operation  $\varphi_{u,v}$  transforms an order- $p$  tensor  $\mathbf{A}$  with a shape  $\mathbf{n}$  and layout  $\boldsymbol{\pi}$  tuple to an order- $p'$  view  $\mathbf{B}$  with a shape  $\mathbf{m}$  and layout  $\boldsymbol{\tau}$  tuple of length  $p'$  with  $p' = p - v + u$  and  $1 \leq u < v \leq p$ . It is akin to tensor unfolding, also known as matricization and vectorization [4, p.459]. However, it neither modifies the element ordering nor copies tensor elements. Given a layout tuple

$\boldsymbol{\pi}$  of  $\mathbf{A}$ , the flattening operation  $\varphi_{u,v}$  is defined for contiguous modes  $\hat{\boldsymbol{\pi}} = (\pi_u, \pi_{u+1}, \dots, \pi_v)$  of  $\boldsymbol{\pi}$ . With  $j_k = 0$  if  $k \leq u$  and  $j_k = v - u$  if  $k > u$  where  $1 \leq k \leq p'$ , the resulting layout tuple  $\boldsymbol{\tau} = (\tau_1, \dots, \tau_{p'})$  of  $\mathbf{B}$  is then given by  $\tau_u = \min(\boldsymbol{\pi}_{u,v})$  and  $\tau_k = \pi_{k+j_k} - s_k$  for  $k \neq u$  with  $s_k = |\{\pi_i \mid \pi_{k+j_k} > \pi_i \wedge \pi_i \neq \min(\hat{\boldsymbol{\pi}}) \wedge u \leq i \leq v\}|$ . Elements of the shape tuple  $\mathbf{m}$  are defined by  $m_{\tau_u} = \prod_{k=u}^v n_{\pi_k}$  and  $m_{\tau_k} = n_{\pi_{k+j_k}}$  for  $k \neq u$ .

## 4. Algorithm Design

### 4.1. Baseline Algorithm with Contiguous Memory Access

The tensor-times-matrix multiplication in equation 1 can be implemented with one sequential algorithm using a nested recursion [16]. It consists of two **if** statements with an **else** branch that computes a fiber-matrix product with two loops. The outer loop iterates over the dimension  $m$  of  $\mathbf{C}$  and  $\mathbf{B}$ , while the inner iterates over dimension  $n_q$  of  $\mathbf{A}$  and  $\mathbf{B}$  computing an inner product with fibers of  $\mathbf{A}$  and  $\mathbf{B}$ . While matrix  $\mathbf{B}$  can be accessed contiguously depending on its storage format, elements of  $\mathbf{A}$  and  $\mathbf{C}$  are accessed non-contiguously if  $\pi_1 \neq q$ .

A better approach is illustrated in algorithm 1 where the loop order is adjusted to the tensor layout  $\boldsymbol{\pi}$  and memory is accessed contiguously for  $\pi_1 \neq q$  and  $p > 1$ . The adjustment of the loop order is accomplished in line 5 which uses the layout tuple  $\boldsymbol{\pi}$  to select a multi-index element  $i_{\pi_r}$  and to increment it with the corresponding stride  $w_{\pi_r}$ . Hence, with increasing recursion level and decreasing  $r$ , indices are incremented with smaller strides as  $w_{\pi_r} \leq w_{\pi_{r+1}}$ . The second **if** statement in line number 4 allows the loop over mode  $\pi_1$  to be placed into the base case which contains three loops performing a slice-matrix multiplication. In this way, the inner-most loop is able to increment  $i_{\pi_1}$  with a unit stride and contiguously accesses tensor elements of  $\mathbf{A}$  and  $\mathbf{C}$ . The second loop increments  $i_q$  with which elements of  $\mathbf{B}$  are contiguously accessed if  $\mathbf{B}$  is stored in the row-major format. The third loop increments  $j$  and could be placed as the second loop if  $\mathbf{B}$  is stored in the column-major format.

While spatial data locality is improved by adjusting the loop ordering, slices  $\mathbf{A}'_{\pi_1,q}$ , fibers  $\mathbf{C}'_{\pi_1}$  and elements  $\mathbf{B}(j, i_q)$  are accessed  $m$ ,  $n_q$  and  $n_{\pi_1}$  times, respectively. The specified fiber of  $\mathbf{C}$  might fit into first or second level cache, slice elements of  $\mathbf{A}$  are unlikely to fit in the local caches if the slice size  $n_{\pi_1} \times n_q$  is large, leading to higher cache misses and suboptimal performance. Instead of optimizing for better temporal data locality, we use existing high-performance BLAS implementations for the base case. The following subsection explains this approach.

### 4.2. BLAS-based Algorithms with Tensor Slices

Algorithm 1 computes the mode- $q$  tensor-matrix product in a recursive fashion for  $p \geq 2$  and  $\pi_1 \neq q$  where its base case multiplies different tensor slices of  $\mathbf{A}$  with the

---

```

1  ttm(A, B, C, n,  $\pi$ , i,  $m$ ,  $q$ ,  $\hat{q}$ ,  $r$ )
2  if  $r = \hat{q}$  then
3    ttm(A, B, C, n,  $\pi$ , i,  $m$ ,  $q$ ,  $\hat{q}$ ,  $r - 1$ )
4  else if  $r > 1$  then
5    for  $i_{\pi_r} \leftarrow 1$  to  $n_{\pi_r}$  do
6      ttm(A, B, C, n,  $\pi$ , i,  $m$ ,  $q$ ,  $\hat{q}$ ,  $r - 1$ )
7  else
8    for  $j \leftarrow 1$  to  $m$  do
9      for  $i_q \leftarrow 1$  to  $n_q$  do
10       for  $i_{\pi_1} \leftarrow 1$  to  $n_{\pi_1}$  do
11          $\underline{C}([i_1, j, i_2]) += \underline{A}([i_1, i_q, i_2]) \cdot \mathbf{B}(j, i_q)$ 

```

---

**Algorithm 1:** Modified baseline algorithm with contiguous memory access for the tensor-matrix multiplication. The tensor order  $p$  must be greater than 1 and the contraction mode  $q$  must satisfy  $1 \leq q \leq p$  and  $\pi_1 \neq q$ . The initial call must happen with  $r = p$  where  $\mathbf{n}$  is the shape tuple of  $\underline{\mathbf{A}}$  and  $m$  is the  $q$ -th dimension of  $\underline{\mathbf{C}}$ .

matrix  $\mathbf{B}$ . Instead of optimizing the slice-matrix multiplication in the base case, one can use a CBLAS `gemm` function instead<sup>1</sup>. The latter denotes a general matrix-matrix multiplication which is defined as  $\mathbf{C} := \mathbf{a} * \text{op}(\mathbf{A}) * \text{op}(\mathbf{B}) + \mathbf{b} * \mathbf{C}$  where  $\mathbf{a}$  and  $\mathbf{b}$  are scalars,  $\mathbf{A}$ ,  $\mathbf{B}$  and  $\mathbf{C}$  are matrices,  $\text{op}(\mathbf{A})$  is an  $M$ -by- $K$  matrix,  $\text{op}(\mathbf{B})$  is a  $K$ -by- $N$  matrix and  $\mathbf{C}$  is an  $N$ -by- $N$  matrix. Function  $\text{op}(\mathbf{x})$  either transposes the corresponding matrix  $\mathbf{x}$  such that  $\text{op}(\mathbf{x}) = \mathbf{x}'$  or not  $\text{op}(\mathbf{x}) = \mathbf{x}$ .

For  $\pi_1 = q$ , the tensor-matrix product can be computed by a matrix-matrix multiplication where the input tensor  $\underline{\mathbf{A}}$  can be flattened into a matrix without any copy operation. The same can be applied when  $\pi_p = q$  and five other cases where the input tensor is either one or two-dimensional. In summary, there are seven other corner cases to the general case where a single `gemv` or `gemm` call suffices to compute the tensor-matrix product. All eight cases per storage format are listed in table 1. The arguments of the routines `gemv` or `gemm` are set according to the tensor order  $p$ , tensor layout  $\pi$  and contraction mode  $q$ . If the input matrix  $\mathbf{B}$  has the row-major order, parameter `CBLAS_ORDER` of function `gemm` is set to `CblasRowMajor` (`rm`) and `CblasColMajor` (`cm`) otherwise. Note that table 1 supports all linear tensor layouts of  $\underline{\mathbf{A}}$  and  $\underline{\mathbf{C}}$  with no limitations on tensor order and contraction mode. The following subsection describes all eight cases when the input matrix  $\mathbf{B}$  has the row-major ordering.

Note that the CBLAS also allows users to specify matrix's leading dimension by providing the `LDA`, `LDB` and `LDC` parameters. A leading dimension determines the number of elements that is required for iterating over the non-contiguous matrix dimension. The additional parameter enables the matrix multiplication to be performed with submatrices or even fibers within submatrices. The leading dimension parameter is necessary for implementing a BLAS-based tensor-matrix multiplication with subtensors and tensor slices.

<sup>1</sup>CBLAS denotes the C interface to the BLAS.

#### 4.2.1. Row-Major Matrix Multiplication

*Case 1:* If  $p = 1$ , The tensor-vector product  $\underline{\mathbf{A}} \times_1 \mathbf{B}$  can be computed with a `gemv` operation where  $\underline{\mathbf{A}}$  is an order-1 tensor  $\mathbf{a}$  of length  $n_1$  such that  $\mathbf{a}^T \cdot \mathbf{B}$ .

*Case 2-5:* If  $p = 2$ ,  $\underline{\mathbf{A}}$  and  $\underline{\mathbf{C}}$  are order-2 tensors with dimensions  $n_1$  and  $n_2$ . In this case the tensor-matrix product can be computed with a single `gemm`. If  $\mathbf{A}$  and  $\mathbf{C}$  have the column-major format with  $\pi = (1, 2)$ , `gemm` either executes  $\mathbf{C} = \mathbf{A} \cdot \mathbf{B}^T$  for  $q = 1$  or  $\mathbf{C} = \mathbf{B} \cdot \mathbf{A}$  for  $q = 2$ . Both matrices can be interpreted  $\mathbf{C}$  and  $\mathbf{A}$  as matrices in row-major format although both are stored column-wise. If  $\mathbf{A}$  and  $\mathbf{C}$  have the row-major format with  $\pi = (2, 1)$ , `gemm` either executes  $\mathbf{C} = \mathbf{B} \cdot \mathbf{A}$  for  $q = 1$  or  $\mathbf{C} = \mathbf{A} \cdot \mathbf{B}^T$  for  $q = 2$ . The transposition of  $\mathbf{B}$  is necessary for the cases 2 and 5 which is independent of the chosen layout.

*Case 6-7 :* If  $p > 2$  and if  $q = \pi_1$  (case 6), a single `gemm` with the corresponding arguments executes  $\mathbf{C} = \mathbf{A} \cdot \mathbf{B}^T$  and computes a tensor-matrix product  $\underline{\mathbf{C}} = \underline{\mathbf{A}} \times_{\pi_1} \mathbf{B}$ . Tensors  $\underline{\mathbf{A}}$  and  $\underline{\mathbf{C}}$  are flattened with  $\varphi_{2,p}$  to row-major matrices  $\mathbf{A}$  and  $\mathbf{C}$ . Matrix  $\mathbf{A}$  has  $\bar{n}_{\pi_1} = \bar{n}/n_{\pi_1}$  rows and  $n_{\pi_1}$  columns while matrix  $\mathbf{C}$  has the same number of rows and  $m$  columns. If  $\pi_p = q$  (case 7),  $\underline{\mathbf{A}}$  and  $\underline{\mathbf{C}}$  are flattened with  $\varphi_{1,p-1}$  to column-major matrices  $\mathbf{A}$  and  $\mathbf{C}$ . Matrix  $\mathbf{A}$  has  $n_{\pi_p}$  rows and  $\bar{n}_{\pi_p} = \bar{n}/n_{\pi_p}$  columns while  $\mathbf{C}$  has  $m$  rows and the same number of columns. In this case, a single `gemm` executes  $\mathbf{C} = \mathbf{B} \cdot \mathbf{A}$  and computes  $\underline{\mathbf{C}} = \underline{\mathbf{A}} \times_{\pi_p} \mathbf{B}$ . Noticeably, the desired contraction are performed without copy operations, see subsection 3.5.

*Case 8 ( $p > 2$ ):* If the tensor order is greater than 2 with  $\pi_1 \neq q$  and  $\pi_p \neq q$ , the modified baseline algorithm 1 is used to successively call  $\bar{n}/(n_q \cdot n_{\pi_1})$  times `gemm` with different tensor slices of  $\underline{\mathbf{C}}$  and  $\underline{\mathbf{A}}$ . Each `gemm` computes one slice  $\underline{\mathbf{C}}'_{\pi_1,q}$  of the tensor-matrix product  $\underline{\mathbf{C}}$  using the corresponding tensor slices  $\underline{\mathbf{A}}'_{\pi_1,q}$  and the matrix  $\mathbf{B}$ . The matrix-matrix product  $\mathbf{C} = \mathbf{B} \cdot \mathbf{A}$  is performed by interpreting both tensor slices as row-major matrices  $\mathbf{A}$  and  $\mathbf{C}$  which have the dimensions  $(n_q, n_{\pi_1})$  and  $(m, n_{\pi_1})$ , respectively.

#### 4.2.2. Column-Major Matrix Multiplication

The tensor-matrix multiplication is performed with the column-major version of `gemm` when the input matrix  $\mathbf{B}$  is stored in column-major order. Although the number of `gemm` cases remains the same, the `gemm` arguments must be rearranged. The argument arrangement for the column-major version can be derived from the row-major version that is provided in table 1.

Firstly, the BLAS arguments of `M` and `N`, as well as `A` and `B` must be swapped. Additionally, the transposition flag for matrix  $\mathbf{B}$  is toggled. Also, the leading dimension argument of  $\mathbf{A}$  is swapped to `LDB` or `LDA`. The only new argument is the new leading dimension of  $\mathbf{B}$ .

Given case 4 with the row-major matrix multiplication in table 1 where tensor  $\underline{\mathbf{A}}$  and matrix  $\mathbf{B}$  are passed to `B` and `A`. The corresponding column-major version is attained when tensor  $\underline{\mathbf{A}}$  and matrix  $\mathbf{B}$  are passed to `A` and

Case	Order $p$	Layout $\pi_{\underline{\mathbf{A}}, \underline{\mathbf{C}}}$	Layout $\pi_{\mathbf{B}}$	Mode $q$	Routine	T	M	N	K	A	LDA	B	LDB	LDC
1	1	-	rm/cm	1	gemv	-	$m$	$n_1$	-	$\underline{\mathbf{B}}$	$n_1$	$\underline{\mathbf{A}}$	-	-
2	2	cm	rm	1	gemm	$\mathbf{B}$	$n_2$	$m$	$n_1$	$\underline{\mathbf{A}}$	$n_1$	$\mathbf{B}$	$n_1$	$m$
	2	cm	cm	1	gemm	-	$m$	$n_2$	$n_1$	$\underline{\mathbf{B}}$	$m$	$\underline{\mathbf{A}}$	$n_1$	$m$
3	2	cm	rm	2	gemm	-	$m$	$n_1$	$n_2$	$\mathbf{B}$	$n_2$	$\underline{\mathbf{A}}$	$n_1$	$n_1$
	2	cm	cm	2	gemm	$\mathbf{B}$	$n_1$	$m$	$n_2$	$\underline{\mathbf{A}}$	$n_1$	$\mathbf{B}$	$m$	$n_1$
4	2	rm	rm	1	gemm	-	$m$	$n_2$	$n_1$	$\underline{\mathbf{B}}$	$n_1$	$\underline{\mathbf{A}}$	$n_2$	$n_2$
	2	rm	cm	1	gemm	$\mathbf{B}$	$n_2$	$m$	$n_1$	$\underline{\mathbf{A}}$	$n_2$	$\mathbf{B}$	$m$	$n_2$
5	2	rm	rm	2	gemm	$\mathbf{B}$	$n_1$	$m$	$n_2$	$\underline{\mathbf{A}}$	$n_2$	$\mathbf{B}$	$n_2$	$m$
	2	rm	cm	2	gemm	-	$m$	$n_1$	$n_2$	$\underline{\mathbf{B}}$	$m$	$\underline{\mathbf{A}}$	$n_2$	$m$
6	$> 2$	any	rm	$\pi_1$	gemm	$\mathbf{B}$	$\bar{n}_q$	$m$	$n_q$	$\underline{\mathbf{A}}$	$n_q$	$\mathbf{B}$	$n_q$	$m$
	$> 2$	any	cm	$\pi_1$	gemm	-	$m$	$\bar{n}_q$	$n_q$	$\underline{\mathbf{B}}$	$m$	$\underline{\mathbf{A}}$	$n_q$	$m$
7	$> 2$	any	rm	$\pi_p$	gemm	-	$m$	$\bar{n}_q$	$n_q$	$\mathbf{B}$	$n_q$	$\underline{\mathbf{A}}$	$\bar{n}_q$	$\bar{n}_q$
	$> 2$	any	cm	$\pi_p$	gemm	$\mathbf{B}$	$\bar{n}_q$	$m$	$n_q$	$\underline{\mathbf{A}}$	$\bar{n}_q$	$\mathbf{B}$	$m$	$\bar{n}_q$
8	$> 2$	any	rm	$\pi_2, \dots, \pi_{p-1}$	gemm*	-	$m$	$n_{\pi_1}$	$n_q$	$\underline{\mathbf{B}}$	$n_q$	$\underline{\mathbf{A}}$	$w_q$	$w_q$
	$> 2$	any	cm	$\pi_2, \dots, \pi_{p-1}$	gemm*	$\mathbf{B}$	$n_{\pi_1}$	$m$	$n_q$	$\underline{\mathbf{A}}$	$w_q$	$\mathbf{B}$	$m$	$w_q$

Table 1: Eight cases of CBLAS functions `gemm` and `gemv` implementing the mode- $q$  tensor-matrix multiplication with a row-major or column-major format. Arguments T, M, N, etc. of `gemv` and `gemm` are chosen with respect to the tensor order  $p$ , layout  $\pi$  of  $\underline{\mathbf{A}}$ ,  $\mathbf{B}$ ,  $\underline{\mathbf{C}}$  and contraction mode  $q$  where T specifies if  $\mathbf{B}$  is transposed. Function `gemm*` with a star denotes multiple `gemm` calls with different tensor slices. Argument  $\bar{n}_q$  for case 6 and 7 is defined as  $\bar{n}_q = (\prod_r n_r)/n_q$ . Input matrix  $\mathbf{B}$  is either stored in the column-major or row-major format. The storage format flag set for `gemm` and `gemv` is determined by the element ordering of  $\mathbf{B}$ .

$\mathbf{B}$  where the transpose flag for  $\mathbf{B}$  is set and the remaining dimensions are adjusted accordingly.

#### 4.2.3. Matrix Multiplication Variations

The column-major and row-major versions of `gemm` can be used interchangeably by adapting the storage format. This means that a `gemm` operation for column-major matrices can compute the same matrix product as one for row-major matrices, provided that the arguments are rearranged accordingly. While the argument rearrangement is similar, the arguments associated with the matrices  $\mathbf{A}$  and  $\mathbf{B}$  must be interchanged. Specifically, LDA and LDB as well as M and N are swapped along with the corresponding matrix pointers. In addition, the transposition flag must be set for  $\mathbf{A}$  or  $\mathbf{B}$  in the new format if  $\mathbf{B}$  or  $\mathbf{A}$  is transposed in the original version.

For instance, the column-major matrix multiplication in case 4 of table 1 requires the arguments of  $\mathbf{A}$  and  $\mathbf{B}$  to be tensor  $\underline{\mathbf{A}}$  and matrix  $\mathbf{B}$  with  $\mathbf{B}$  being transposed. The arguments of an equivalent row-major multiplication for  $\mathbf{A}$ ,  $\mathbf{B}$ , M, N, LDA, LDB and T are then initialized with  $\mathbf{B}$ ,  $\underline{\mathbf{A}}$ ,  $m$ ,  $n_2$ ,  $m$ ,  $n_2$  and  $\mathbf{B}$ .

Another possible matrix multiplication variant with the same product is computed when, instead of  $\mathbf{B}$ , tensors  $\underline{\mathbf{A}}$  and  $\underline{\mathbf{C}}$  with adjusted arguments are transposed. We assume that such reformulations of the matrix multiplication do not outperform the variants shown in Table 1, as we expect highly optimized BLAS libraries to adjust

#### 4.3. Matrix Multiplication with Subtensors

Algorithm 1 can be slightly modified in order to call `gemm` with flattened order- $\hat{q}$  subtensors that correspond to larger tensor slices. Given the contraction mode  $q$  with  $1 < q < p$ , the maximum number of additionally fusible

modes is  $\hat{q} - 1$  with  $\hat{q} = \pi^{-1}(q)$  where  $\pi^{-1}$  is the inverse layout tuple. The corresponding fusible modes are therefore  $\pi_1, \pi_2, \dots, \pi_{\hat{q}-1}$ .

The non-base case of the modified algorithm only iterates over dimensions that have indices larger than  $\hat{q}$  and thus omitting the first  $\hat{q}$  modes. The conditions in line 2 and 4 are changed to  $1 < r \leq \hat{q}$  and  $\hat{q} < r$ , respectively. Thus, loop indices belonging to the outer  $\pi_r$ -th loop with  $\hat{q} + 1 \leq r \leq p$  define the order- $\hat{q}$  subtensors  $\underline{\mathbf{A}}'_{\pi'}$  and  $\underline{\mathbf{C}}'_{\pi'}$  of  $\underline{\mathbf{A}}$  and  $\underline{\mathbf{C}}$  with  $\pi' = (\pi_1, \dots, \pi_{\hat{q}-1}, q)$ . Flattening the subtensors  $\underline{\mathbf{A}}'_{\pi'}$  and  $\underline{\mathbf{C}}'_{\pi'}$  with  $\varphi_{1, \hat{q}-1}$  for the modes  $\pi_1, \dots, \pi_{\hat{q}-1}$  yields two tensor slices with dimension  $n_q$  or  $m$  and the fused dimension  $\bar{n}_q = \prod_{r=1}^{\hat{q}-1} n_{\pi_r}$  with  $\bar{n}_q = w_q$ . Both tensor slices can be interpreted either as row-major or column-major matrices with shapes  $(n_q, \bar{n}_q)$  or  $(w_q, \bar{n}_q)$  in case of  $\underline{\mathbf{A}}$  and  $(m, \bar{n}_q)$  or  $(\bar{n}_q, m)$  in case of  $\underline{\mathbf{C}}$ , respectively.

The `gemm` function in the base case is called with almost identical arguments except for the parameter  $M$  or  $N$  which is set to  $\bar{n}_q$  for a column-major or row-major multiplication, respectively. Note that neither the selection of the subtensor nor the flattening operation copy tensor elements. This description supports all linear tensor layouts and generalizes lemma 4.2 in [10] without copying tensor elements, see section 3.5.

#### 4.4. Parallel BLAS-based Algorithms

Most BLAS libraries allow to change the number of threads. Hence, functions such as `gemm` and `gemv` can be run either using a single or multiple threads. The TTM cases one to seven contain a single BLAS call which is why we set the number of threads to the number of available cores. The following subsections discuss parallel versions for the eighth case in which the outer loops of algorithm 1 and the `gemm` function inside the base case can be run

---

```

1 ttm<par-loop><slice>(A, B, C, n,  $\pi$ ,  $m$ ,  $q$ ,  $p$ )
2   [A', C', n', w'] = flatten(A, C, n,  $m$ ,  $\pi$ ,  $q$ ,  $p$ )
3   parallel for  $i \leftarrow 1$  to  $n'_4$  do
4     parallel for  $j \leftarrow 1$  to  $n'_2$  do
5       gemm( $m$ ,  $n'_1$ ,  $n'_3$ , 1, B,  $n'_3$ , A' $ij$ ,  $w'_3$ , 0, C' $ij$ ,  $w'_3$ )

```

---

**Algorithm 2:** Function `ttm<par-loop><slice>` is an optimized version of Algorithm 1. The `flatten` function transforms the order- $p$  tensors **A** and **C** with layout tuple  $\pi$  and their respective dimension tuples **n** and **m** into order-4 tensors **A'** and **C'** with layout tuple  $\pi'$  and their respective dimension tuples **n'** and **m'** where  $\mathbf{n}' = (n_{\pi_1}, \hat{n}_{\pi_2}, n_q, \hat{n}_{\pi_4})$  and  $m'_3 = m$  and  $n'_k = m'_k$  for  $k \neq 3$ . Each thread calls multiple single-threaded `gemm` functions each of which executes a slice-matrix multiplication with the order-2 tensor slices **A'** <sub>$ij$</sub>  and **C'** <sub>$ij$</sub> . Matrix **B** has the row-major storage format.

in parallel. Note that the parallelization strategies can be combined with the aforementioned slicing methods.

#### 4.4.1. Sequential Loops and Parallel Matrix Multiplication

Algorithm 1 is run for the eighth case and does not need to be modified except for enabling `gemm` to run multi-threaded in the base case. This type of parallelization strategy might be beneficial with order- $\hat{q}$  subtensors where the contraction mode satisfies  $q = \pi_{p-1}$ , the inner dimensions  $n_{\pi_1}, \dots, n_{\hat{q}}$  are large and the outer-most dimension  $n_{\pi_p}$  is smaller than the available processor cores. For instance, given a first-order storage format and the contraction mode  $q$  with  $q = p - 1$  and  $n_p = 2$ , the dimensions of flattened order- $q$  subtensors are  $\prod_{r=1}^{p-2} n_r$  and  $n_{p-1}$ . This allows `gemm` to be executed with large dimensions using multiple threads increasing the likelihood to reach a high throughput. However, if the above conditions are not met, a multi-threaded `gemm` operates on small tensor slices which might lead to an suboptimal utilization of the available cores. This algorithm version will be referred to as `<par-gemm>`. Depending on the subtensor shape, we will either add `<slice>` for order-2 subtensors or `<subtensor>` for order- $\hat{q}$  subtensors with  $\hat{q} = \pi_q^{-1}$ .

#### 4.4.2. Parallel Loops and Sequential Matrix Multiplication

Instead of sequentially calling multi-threaded `gemm`, it is also possible to call single-threaded `gemms` in parallel. Similar to the previous approach, the matrix multiplication can be performed with tensor slices or order- $\hat{q}$  subtensors.

**Matrix Multiplication with Tensor Slices.** Algorithm 2 with function `ttm<par-loop><slice>` executes a single-threaded `gemm` with tensor slices in parallel using all modes except  $\pi_1$  and  $\pi_{\hat{q}}$ . The first statement of the algorithm calls the `flatten` function which transforms tensors **A** and **C** without copying elements by calling the flattening operation  $\varphi_{\pi_{\hat{q}+1}, \pi_p}$  and  $\varphi_{\pi_2, \pi_{\hat{q}-1}}$ . The resulting tensors **A'** and **C'** are of order 4. Tensor **A'** has the shape  $\mathbf{n}' = (n_{\pi_1}, \hat{n}_{\pi_2}, n_q, \hat{n}_{\pi_4})$  with the dimensions  $\hat{n}_{\pi_2} = \prod_{r=2}^{\hat{q}-1} n_{\pi_r}$  and  $\hat{n}_{\pi_4} = \prod_{r=\hat{q}+1}^p n_{\pi_r}$ . Tensor **C'** has the same shape as

**A'** with dimensions  $m'_r = n'_r$  except for the third dimension which is given by  $m_3 = m$ .

The following two `parallel for` loop constructs index all free modes. The outer loop iterates over  $n'_4 = \hat{n}_{\pi_4}$  while the inner one loops over  $n'_2 = \hat{n}_{\pi_2}$  calling `gemm` with tensor slices **A'** <sub>$2,4$</sub>  and **C'** <sub>$2,4$</sub> . Here, we assume that matrix **B** has the row-major format which is why both tensor slices are also treated as row-major matrices. Notice that `gemm` in Algorithm 2 will be called with exact same arguments as displayed in the eighth case in table 1 where  $n'_1 = n_{\pi_1}$ ,  $n'_3 = n_q$  and  $w_q = w'_3$ . For the sake of simplicity, we omitted the first three arguments of `gemm` which are set to `CblasRowMajor` and `CblasNoTrans` for **A** and **B**. With the help of the flattening operation, the tree-recursion has been transformed into two loops which iterate over all free indices.

**Matrix Multiplication with Subtensors.** The following algorithm and the flattening of subtensors is a combination of the previous paragraph and subsection 4.3. With order- $\hat{q}$  subtensors, only the outer modes  $\pi_{\hat{q}+1}, \dots, \pi_p$  are free for parallel execution while the inner modes  $\pi_1, \dots, \pi_{\hat{q}-1}, q$  are used for the slice-matrix multiplication. Therefore, both tensors are flattened twice using the flattening operations  $\varphi_{\pi_1, \pi_{\hat{q}-1}}$  and  $\varphi_{\pi_{\hat{q}+1}, \pi_p}$ . Note that in contrast to tensor slices, the first flattening also contains the dimension  $n_{\pi_1}$ . The flattened tensors are of order 3 where **A'** has the shape  $\mathbf{n}' = (\hat{n}_{\pi_1}, n_q, \hat{n}_{\pi_3})$  with  $\hat{n}_{\pi_1} = \prod_{r=1}^{\hat{q}-1} n_{\pi_r}$  and  $\hat{n}_{\pi_3} = \prod_{r=\hat{q}+1}^p n_{\pi_r}$ . Tensor **C'** has the same dimensions as **A'** except for  $m_2 = m$ .

Algorithm 2 needs a minor modification for supporting order- $\hat{q}$  subtensors. Instead of two loops, the modified algorithm consists of a single loop which iterates over dimension  $\hat{n}_{\pi_3}$  calling a single-threaded `gemm` with subtensors **A'** and **C'**. The shape and strides of both subtensors as well as the function arguments of `gemm` have already been provided by the previous subsection 4.3. This `ttm` version will be referred to as `<par-loop><subtensor>`.

Note that functions `<par-gemm>` and `<par-loop>` implement opposing versions of the `ttm` where either `gemm` or the fused loop is performed in parallel. Version `<par-loop-gemm>` executes available loops in parallel where each loop thread executes a multi-threaded `gemm` with either subtensors or tensor slices.

#### 4.4.3. Combined Matrix Multiplication

The combined matrix multiplication calls one of the previously discussed functions depending on the number of available cores. The heuristic is designed under the assumption that function `<par-gemm>` is not able to efficiently utilize the processor cores if subtensors or tensor slices are too small. The corresponding algorithm switches between `<par-loop>` and `<par-gemm>` with subtensors by first calculating the parallel and combined loop count  $\hat{n} = \prod_{r=1}^{\hat{q}-1} n_{\pi_r}$  and  $\hat{n}' = \prod_{r=1}^p n_{\pi_r} / n_q$ , respectively. Given number of physical processor cores as `ncores`, the algorithm executes `<par-loop>` with `<subtensor>` if `ncores` is greater than or

equal to  $\hat{n}$  and call `<par-loop>` with `<slice>` if `ncores` is greater than or equal to  $\hat{n}'$ . Otherwise, the algorithm will default to `<par-gemm>` with `<subtensor>`. Function `par-gemm` with tensor slices is not used here. The presented strategy is different to the one presented in [10] that maximizes the number of modes involved in the matrix multiply. We will refer to this version as `<combined>` to denote a selected combination of `<par-loop>` and `<par-gemm>` functions.

#### 4.4.4. Multithreaded Batched Matrix Multiplication

The multithreaded batched matrix multiplication version calls in the eighth case a single `gemm_batch` function that is provided by Intel MKL’s BLAS-like extension. With an interface that is similar to the one of `cblas_gemm`, function `gemm_batch` performs a series of matrix-matrix operations with general matrices. All parameters except `CBLAS_LAYOUT` requires an array as an argument which is why different subtensors of the same corresponding tensors are passed to `gemm_batch`. The subtensor dimensions and remaining `gemm` arguments are replicated within the corresponding arrays. Note that the MKL is responsible of how subtensor-matrix multiplications are executed and whether subtensors are further divided into smaller subtensors or tensor slices. This algorithm will be referred to as `<mk1-batch-gemm>`.

## 5. Experimental Setup

### 5.1. Computing System

The experiments have been carried out on a dual socket Intel Xeon Gold 5318Y CPU with an Ice Lake architecture and a dual socket AMD EPYC 9354 CPU with a Zen4 architecture. With two NUMA domains, the Intel CPU consists of  $2 \times 24$  cores which run at a base frequency of 2.1 GHz. Assuming peak AVX-512 Turbo frequency of 2.5 GHz, the CPU is able to process 3.84 TFLOPS in double precision. Using the Likwid performance tool, we measured a peak double-precision floating-point performance of 3.8043 TFLOPS (79.25 GFLOPS/core) and a peak memory throughput of 288.68 GB/s. The AMD CPU consists of  $2 \times 32$  cores running at a base frequency of 3.25 GHz. Assuming an all-core boost frequency of 3.75 GHz, the CPU is theoretically capable of performing 3.84 TFLOPS in double precision. Using the Likwid performance tool, we measured a peak double-precision floating-point performance of 3.87 TFLOPS (60.5 GFLOPS/core) and a peak memory throughput of 788.71 GB/s.

We have used the GNU compiler v11.2.0 with the highest optimization level `-O3` together with the `-fopenmp` and `-std=c++17` flags. Loops within the eighth case have been parallelized using GCC’s OpenMP v4.5 implementation. In case of the Intel CPU, the 2022 Intel Math Kernel Library (MKL) and its threading library `mk1_intel_thread` together with the threading runtime library `libiomp5` has been used for the three BLAS functions `gemv`, `gemm` and

`gemm_batch`. For the AMD CPU, we have compiled AMD AOCL v4.2.0 together with set the `zen4` architecture configuration option and enabled OpenMP threading.

### 5.2. OpenMP Parallelization

The two `parallel for` loops have been parallelized using the OpenMP directive `omp parallel for` together with the `schedule(static)`, `num_threads(ncores)` and `proc_bind(spread)` clauses. In case of tensor-slices, the `collapse(2)` clause is added for transforming both loops into one loop which has an iteration space of the first loop times the second one.

The `num_threads(ncores)` clause specifies the number of threads within a team where `ncores` is equal to the number of processor cores. Hence, each OpenMP thread is responsible for computing  $\bar{n}'/\text{ncores}$  independent slice-matrix products where  $\bar{n}' = n_2' \cdot n_4'$  for tensor slices and  $\bar{n}' = n_4'$  for mode- $\hat{q}$  subtensors.

The `schedule(static)` instructs the OpenMP runtime to divide the iteration space into almost equally sized chunks. Each thread sequentially computes  $\bar{n}'/\text{ncores}$  slice-matrix products. We decided to use this scheduling kind as all slice-matrix multiplications have the same number of floating-point operations with a regular workload where one can assume negligible load imbalance. Moreover, we wanted to prevent scheduling overheads for small slice-matrix products where data locality can be an important factor for achieving higher throughput.

We did not set the `OMP_PLACES` environment variable which defaults to the OpenMP `cores` setting defining a place as a single processor core. Together with the clause `num_threads(ncores)`, the number of OpenMP threads is equal to the number of OpenMP places, i.e. to the number of processor cores. We did not measure any performance improvements for a higher thread count.

The `proc_bind(spread)` clause additionally binds each OpenMP thread to one OpenMP place which lowers inter-node or inter-socket communication and improves local memory access. Moreover, with the `spread` thread affinity policy, consecutive OpenMP threads are spread across OpenMP places which can be beneficial if the user decides to set `ncores` smaller than the number of processor cores.

### 5.3. Tensor Shapes

We have used asymmetrically and symmetrically shaped tensors in order to cover many use cases. The dimension tuples of both shape types are organized within two three-dimensional arrays with which tensors are initialized. The dimension array for the first shape type contains  $720 = 9 \times 8 \times 10$  dimension tuples where the row number is the tensor order ranging from 2 to 10. For each tensor order, 8 tensor instances with increasing tensor size is generated. A special feature of this test set is that the contraction dimension and the leading dimension are disproportionately large. The second set consists of  $336 = 6 \times 8 \times 7$  dimensions tuples where the tensor order

625 ranges from 2 to 7 and has 8 dimension tuples for each  
 626 order. Each tensor dimension within the second set is  $2^{12}$ ,  
 627  $2^8$ ,  $2^6$ ,  $2^5$ ,  $2^4$  and  $2^3$ . A detailed explanation of the tensor  
 628 shape setup is given in [12, 16].

629 If not otherwise mentioned, both tensors **A** and **C** are  
 630 stored according to the first-order tensor layout. Matrix  
 631 **B** has the row-major storage format.

## 632 6. Results and Discussion

### 633 6.1. Slicing Methods

634 This section analyzes the performance of the two pro-  
 635 posed slicing methods `<slice>` and `<subtensor>` that have  
 636 been discussed in section 4.4. Figure 1 contains eight per-  
 637 formance contour plots of four `ttm` functions `<par-loop>`  
 638 and `<par-gemm>` that either compute the slice-matrix prod-  
 639 uct with subtensors `<subtensor>` or tensor slices `<slice>`.  
 640 Each contour level within the plots represents a mean  
 641 GFLOPS/core value that is averaged across tensor sizes.

642 Moreover, each contour plot contains all applicable TTM  
 643 cases listed in Table 1. The first column of performance  
 644 values is generated by `gemm` belonging to case 3, except the  
 645 first element which corresponds to case 2. The first row,  
 646 excluding the first element, is generated by case 6 function.  
 647 Case 7 is covered by the diagonal line of performance val-  
 648 ues when  $q = p$ . Although Figure 1 suggests that  $q > p$   
 649 is possible, our profiling program sets  $q = p$ . Finally, case  
 650 8 with multiple `gemm` calls is represented by the triangular  
 651 region which is defined by  $1 < q < p$ .

652 Function `<par-loop>` with `<slice>` runs on average with  
 653 34.96 GFLOPS/core (1.67 TFLOPS) with asymmetrically  
 654 shaped tensors. With a maximum performance of 57.805  
 655 GFLOPS/core (2.77 TFLOPS), it performs on average  
 656 89.64% faster than function `<par-loop>` with `<subtensor>`.  
 657 The slowdown with subtensors at  $q = p - 1$  or  $q = p - 2$  can  
 658 be explained by the small loop count of the function that  
 659 are 2 and 4, respectively. While function `<par-loop>` with  
 660 tensor slices is affected by the tensor shapes for dimensions  
 661  $p = 3$  and  $p = 4$  as well, its performance improves with  
 662 increasing order due to the increasing loop count.

663 Function `<par-loop>` with tensor slices achieves on av-  
 664 erage 17.34 GFLOPS/core (832.42 GFLOPS) with sym-  
 665 metrically shaped tensors. In this case, `<par-loop>` with  
 666 subtensors achieves a mean throughput of 17.62 GFLOP-  
 667 S/core (846.16 GFLOPS) and is on average 9.89% faster  
 668 than the `<slice>` version. The performances of both func-  
 669 tions are monotonically decreasing with increasing tensor  
 670 order, see plots (1.c) and (1.d) in Figure 1. The average  
 671 performance decrease of both functions can be approxi-  
 672 mated by a cubic polynomial with the coefficients  $-35$ ,  
 673  $640$ ,  $-3848$  and  $8011$ .

674 Function `<par-gemm>` with tensor slices averages 36.42  
 675 GFLOPS/core (1.74 TFLOPS) and achieves up to 57.91  
 676 GFLOPS/core (2.77 TFLOPS) with asymmetrically shaped  
 677 tensors. With subtensors, function `<par-gemm>` exhibits al-  
 678 most identical performance characteristics and is on av-

679 erage only 3.42% slower than its counterpart with tensor  
 680 slices.

681 For symmetrically shaped tensors, `<par-gemm>` with sub-  
 682 tensors and tensor slices achieve a mean throughput 15.98  
 683 GFLOPS/core (767.31 GFLOPS) and 15.43 GFLOPS/-  
 684 core (740.67 GFLOPS), respectively. However, function  
 685 `<par-gemm>` with `<subtensor>` is on average 87.74% faster  
 686 than the `<slice>` which is hardly visible due to small perfor-  
 687 mance values around 5 GFLOPS/core or less whenever  
 688  $q < p$  and the dimensions are smaller than 256. The  
 689 speedup of the `<subtensor>` version can be explained by the  
 690 smaller loop count and slice-matrix multiplications with  
 691 larger tensor slices.

### 692 6.2. Parallelization Methods

693 This section discusses the performance results of the  
 694 two parallelization methods `<par-gemm>` and `<par-loop>` us-  
 695 ing the same Figure 1.

696 With asymmetrically shaped tensors, both `<par-gemm>`  
 697 functions with subtensors and tensor slices compute the  
 698 tensor-matrix product on average between 36 and 37 GFLOP-  
 699 S/core and outperform function `<par-loop><subtensor>` ver-  
 700 sion on average by a factor of 2.31. The speedup can be  
 701 explained by the performance drop of function `<par-loop>`  
 702 `<subtensor>` to 3.49 GFLOPS/core at  $q = p - 1$  while  
 703 both `<par-gemm>` functions operate around 39 GFLOPS/-  
 704 core. Function `<par-loop>` with tensor slices performs bet-  
 705 ter for reasons explained in the previous subsection. It is  
 706 on average 30.57% slower than its `<par-gemm>` version due  
 707 to the aforementioned performance drops.

708 In case of symmetrically shaped tensors, `<par-loop>`  
 709 with subtensors and tensor slices outperform their corre-  
 710 sponding `<par-gemm>` counterparts by 23.3% and 32.9%,  
 711 respectively. The speedup mostly occurs when  $1 < q < p$   
 712 where the performance gain is a factor of 2.23. This per-  
 713 formance behavior can be expected as the tensor slice sizes  
 714 decreases for the eighth case with increasing tensor order  
 715 causing the parallel slice-matrix multiplication to perform  
 716 on smaller matrices. In contrast, `<par-loop>` can execute  
 717 small single-threaded slice-matrix multiplications in par-  
 718 allel.

### 719 6.3. Loops Over Gemm

720 The contour plots in Figure 1 contain performance data  
 721 that are generated by all applicable TTM cases of each  
 722 `ttm` function. Yet, the presented slicing or parallelization  
 723 methods only affect the eighth case, while all other TTM  
 724 cases apply a single multi-threaded `gemm`. The following  
 725 analysis will consider performance values of the eighth case  
 726 in order to have a more fine grained visualization and dis-  
 727 cussion of the loops over `gemm` implementations. Figure 2  
 728 contains cumulative performance distributions of all the  
 729 proposed algorithms including the `<mk1-batch-gemm>` and  
 730 `<combined>` functions for case 8 only. Moreover, the ex-  
 731 periments have been additionally executed on the AMD  
 732 EPYC processor and with the column-major ordering of  
 733 the input matrix as well.



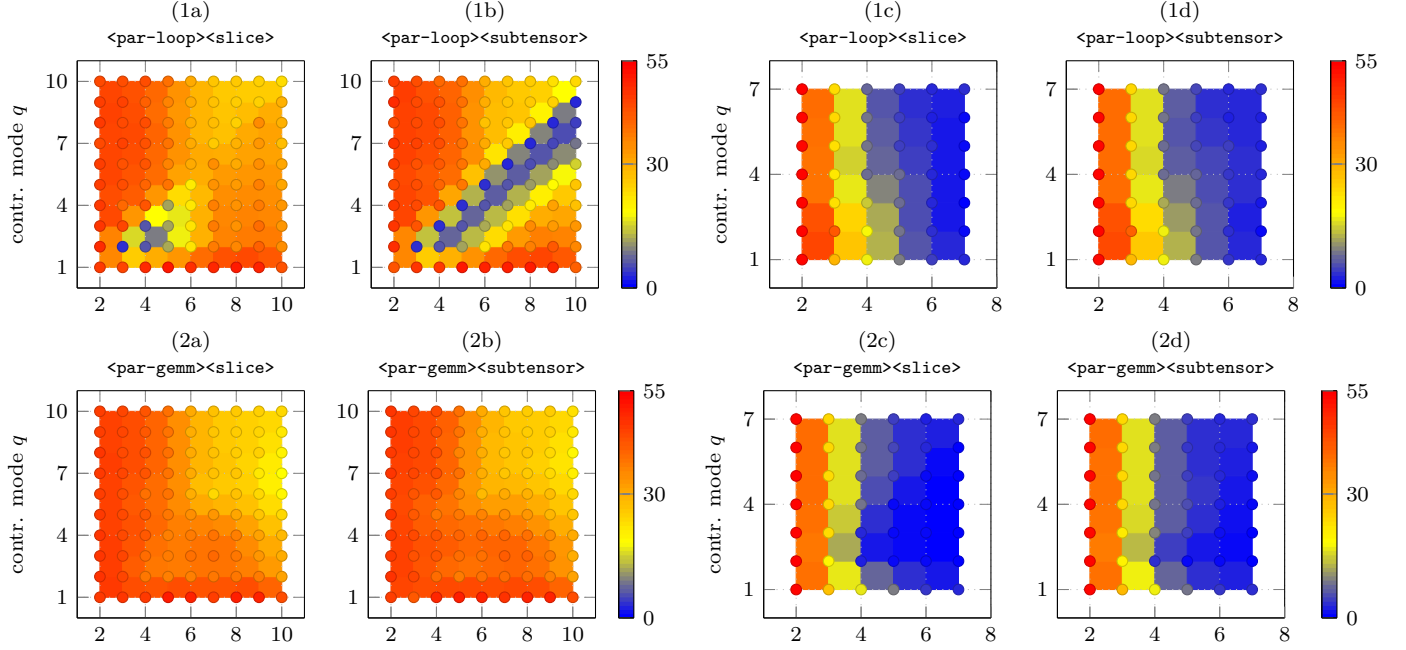


Figure 1: Performance contour plots in double-precision GFLOPS/core of the proposed TTM algorithms `<par-loop>` and `<par-gemm>` with varying tensor orders  $p$  and contraction modes  $q$ . The top row of maps (1x) depict measurements of the `<par-loop>` versions while the bottom row of maps with number (2x) contain measurements of the `<par-gemm>` versions. Tensors are asymmetrically shaped on the left four maps (a,b) and symmetrically shaped on the right four maps (c,d). Tensor  $\underline{A}$  and  $\underline{C}$  have the first-order while matrix  $\underline{B}$  has the row-major ordering. All functions have been measured on an Intel Xeon Gold 5318Y.

Note that the probability  $x$  of a point  $(x, y)$  of a distribution function for a given algorithm corresponds to the number of test instances for which that algorithm achieves a throughput of either  $y$  or less. For instance, function `<mk1-batch-gemm>` computes the tensor-matrix product with asymmetrically shaped tensors in 25% of the tensor instances with equal to or less than 10 GFLOPS/core. Consequently, distribution functions with a logarithmic growth are favorable while exponential behavior is less desirable. Please note that the four plots on the right, plots (c) and (d), have a logarithmic y-axis for a better visualization.

#### 6.3.1. Combined Algorithm and Batched GEMM

Given a row-major matrix ordering, the combined function `<combined>` achieves on the Intel processor a median throughput of 36.15 and 4.28 GFLOPS/core with asymmetrically and symmetrically shaped tensors. Reaching up to 46.96 and 45.68 GFLOPS/core, it is on par with `<par-gemm>` with subtensors and `<par-loop>` with tensor slices and outperforms them for some tensor instances. Note that both functions run significantly slower either with asymmetrically or symmetrically shaped tensors. The observable superior performance distribution of `<combined>` can be explained by its simple heuristic which switches between functions `<par-loop>` and `<par-gemm>` depending on the inner and outer loop count.

Function `<mk1-batch-gemm>` of the BLAS-like extension library has a performance distribution that is very akin to the `<par-loop>` with subtensors. In case of asymmetri-

cally shaped tensors, all functions except `<par-loop>` with subtensors outperform `<mk1-batch-gemm>` on average by a factor of 2.57 and up to a factor 4 for  $2 \leq q \leq 5$  with  $q + 2 \leq p \leq q + 5$ . In contrast, `<par-loop>` with subtensors and `<mk1-batch-gemm>` show a similar performance behavior in the plot (1c) and (1d) for symmetrically shaped tensors, running on average 3.55 and 8.38 times faster than `<par-gemm>` with subtensors and tensor slices, respectively. Function `<par-loop>` with tensor slices underperforms for  $p > 3$ , i.e. when the tensor dimensions are less than 64.

#### 6.3.2. Matrix Formats

The cumulative performance distributions in Figure 2 suggest that the storage format of the input matrix has only a minor impact on the performance. The Euclidean distance between normalized row-major and column-major performance values is around 5 or less with a maximum dissimilarity of 11.61 or 16.97, indicating a moderate similarity between the corresponding row-major and column-major data sets. Moreover, their respective median values with their first and third quartiles differ by less than 5% with three exceptions where the difference of the median values is between 10% and 15% for function `combined` with symmetrically shaped tensors on both processors.

#### 6.3.3. BLAS Libraries

This subsection compares the performance of functions that use Intel's Math Kernel Library (MKL) on the Intel Xeon Gold 5318Y processor with those that use the AMD Optimizing CPU Libraries (AOCL) on the AMD



Figure 2: Cumulative performance distributions in double-precision GFLOPS/core of the proposed algorithms for the eighth case. Each distribution belongs to one algorithm: `<mk1-batch-gemm>` (—), `<combined>` (—), `<par-gemm>` (—) and `<par-loop>` (—) using tensor slices, `<par-gemm>` (—) and `<par-loop>` (—) using subtensors. The top row of maps (1x) depict measurements performed on an Intel Xeon Gold 5318Y with the MKL while the bottom row of maps with number (2x) contain measurements performed on an AMD EPYC 9354 with the AOCL. Tensors are asymmetrically shaped in (a) and (b) and symmetrically shaped in (c) and (d). Input matrix has the row-major ordering (rm) in (a) and (c) and column-major ordering (cm) in (b) and (d).

EPYC 9354 processor. Limiting the performance evaluation to the eighth case, MKL-based functions with asymmetrically shaped tensors run on average between 1.48 and 2.43 times faster than those with the AOCL. For symmetrically shaped tensors, MKL-based functions are between 1.93 and 5.21 times faster than those with the AOCL. In general, MKL-based functions achieve a speedup of at least 1.76 and 1.71 compared to their AOCL-based counterpart when asymmetrically and symmetrically shaped tensors are used.

#### 6.4. Layout-Oblivious Algorithms

Figure 3 contains four subfigures with box plots summarizing the performance distribution of the `<combined>` function using the AOCL and MKL. Every  $k$ th box plot has been computed from benchmark data with symmetrically shaped order-7 tensors that has a  $k$ -order tensor layout. The 1-order and 7-order layout, for instance, are the first-order and last-order storage formats of an order-7 tensor<sup>2</sup>. Note that `<combined>` only calls `<par-loop>` with subtensors only for the .

The reduced performance of around 1 and 2 GFLOPS can be attributed to the fact that contraction and leading dimensions of symmetrically shaped subtensors are at

most 48 and 8, respectively. When `<combined>` is used with MKL, the relative standard deviations (RSD) of its median performances are 2.51% and 0.74%, with respect to the row-major and column-major formats. The RSD of its respective interquartile ranges (IQR) are 4.29% and 6.9%, indicating a similar performance distributions. Using `<combined>` with AOCL, the RSD of its median performances for the row-major and column-major formats are 25.62% and 20.66%, respectively. The RSD of its respective IQRs are 10.83% and 4.31%, indicating a similar performance distributions.

A similar performance behavior can be observed also for other `ttm` variants such as `par-loop` with tensor slices or `par-gemm`. The runtime results demonstrate that the function performances stay within an acceptable range independent for different  $k$ -order tensor layouts and show that our proposed algorithms are not designed for a specific tensor layout.

#### 6.5. Other Approaches

This subsection compares our best performing algorithm with four libraries.

**TCL** implements the TTGT approach with a high-perform tensor-transpose library **HPTT** which is discussed in [7]. **TBLIS** (v1.2.0) implements the GETT approach that is akin to BLIS' algorithm design for the matrix multiplication [8]. The tensor extension of **Eigen** (v3.4.9)

<sup>2</sup>The  $k$ -order tensor layout definition is given in section 3.4



Figure 3: Box plots visualizing performance statics in double-precision GFLOPS/core of `<mk1-batch-gemm>` (left) and `<par-loop>` with subtensors (right). Box plot number  $k$  denotes the  $k$ -order tensor layout of symmetrically shaped tensors with order 7.

is used by the Tensorflow framework. Library **LibTorch** (v2.4.0) is the `c++` distribution of PyTorch [14]. **TLIB** denotes our library using algorithm `<combined>` that have been presented in the previous paragraphs. We will use performance or percentage tuples of the form (TCL, TBLIS, LibTorch, Eigen) where each tuple element denotes the performance or runtime percentage of a particular library.

Figure 2 compares the performance distribution of our implementation with the previously mentioned libraries. Using the MKL on the Intel CPU, our implementation (TLIB) achieves a median performance of 38.21 GFLOPS/core (1.83 TFLOPS) and reaches a maximum performance of 51.65 GFLOPS/core (2.47 TFLOPS) with asymmetrically shaped tensors. It outperforms the competing libraries for almost every tensor instance within the test set. The median library performances are (24.16, 29.85, 28.66, 14.86) GFLOPS/core reaching on average (84.68, 80.61, 78.00, 36.94) percent of TLIB’s throughputs. In case of symmetrically shaped tensors other libraries on the right plot in Figure 2 run at least 2 times slower than TLIB except for TBLIS. TLIB’s median performance is 8.99 GFLOPS/core, other libraries achieve a median performances of (2.70, 9.84, 3.52, 3.80) GFLOPS/core. On average their performances constitute (44.65, 98.63, 53.32, 31.59) percent of TLIB’s throughputs.

On the AMD CPU, our implementation with AOCL computes the tensor-times-matrix product with 24.28 GFLOPS/core (1.55 TFLOPS) and reaches a maximum perfor-

mance of 45.84 GFLOPS/core (2.93 TFLOPS) with asymmetrically shaped tensors. TBLIS reaches 26.81 GFLOPS/core (1.71 TFLOPS) and is slightly faster than TLIB. However, TLIB’s upper performance quartile with 30.82 GFLOPS/core is slightly larger. TLIB outperforms other competing libraries that have a median performance of (8.07, 16.04, 11.49) GFLOPS/core and reach on average (27.97, 62.97, 54.64) percent TLIB’s throughputs. In case of symmetrically shaped tensors, TLIB outperforms all other libraries with 7.52 GFLOPS/core (481.39 GFLOPS) and a maximum performance of 47.78 GFLOPS/core (3.05 TFLOPS). Other libraries perform with (2.03, 6.18, 2.64, 5.58) GFLOPS/core and reach (44.94, 86.67, 57.33, 69.72) percent of TLIB’s throughputs.

While all libraries run on average 25% slower than TLIB across all TTM cases, there are few exceptions. On the AMD CPU, TBLIS reaches 101% of TLIB’s performance for the 6th TTM case and LibTorch performs as fast as TLIB for the 7th TTM case for asymmetrically shaped tensors. One unexpected finding is that LibTorch achieves 96% of TLIB’s performance with asymmetrically shaped tensors and only 28% in case of symmetrically shaped tensors.

On the Intel CPU, LibTorch is on average 9.63% faster than TLIB in the 7th TTM case. The TCL library runs on average as fast as TLIB in the 6th and 7th TTM cases. The performances of TLIB and TBLIS are in the 8th TTM case almost on par, TLIB running about 7.86% faster. In case of symmetrically shaped tensors, all libraries except



Figure 4: Cumulative performance distributions of tensor-times-matrix algorithms in double-precision GFLOPS/core. Each distribution corresponds to a library: **TLIB**[ours] (---), **TCL** (—), **TBLIS** (—), **LibTorch** (—), **Eigen** (—). Libraries have been tested with asymmetrically-shaped (left plot) and symmetrically-shaped tensors (right plot).

Eigen outperform TLIB by about 13%, 42% and 65% in the 7th TTM case. TBLIS and TLIB perform equally well in the 8th TTM case, while other libraries only reach on average 30% of TLIB’s performance. We have also observed that TCL and LibTorch have a median performance of less than 2 GFLOPS/core in the 3rd and 8th TTM case which is less than 6% and 10% of TLIB’s median performance with asymmetrically and symmetrically shaped tensors, respectively. A similar performance behavior can be observed on the AMD CPU.

## 7. Conclusion and Future Work

We presented efficient layout-oblivious algorithms for the compute-bound tensor-matrix multiplication which is essential for many tensor methods. Our approach is based on the LOG-method and computes the tensor-matrix product in-place without transposing tensors. It applies the flexible approach described in [12] and generalizes the findings on tensor slicing in [10] for linear tensor layouts. The resulting algorithms are able to process dense tensors with arbitrary tensor order, dimensions and with any linear tensor layout all of which can be runtime variable.

Our benchmarks show that dividing the base algorithm into eight different TTM cases improves the overall performance. We have demonstrated that algorithms with parallel loops over single-threaded GEMM calls with tensor slices and subtensors perform best. Interestingly, they outperform a single batched GEMM with subtensors, on average, by 14% in case of asymmetrically shaped tensors and if tensor slices are used. Both version computes the

tensor-matrix product on average faster than other state-of-the-art implementations. We have shown that our algorithms are layout-oblivious and do not need further refinement if the tensor layout is changed. We measured a relative standard deviation of 12.95% and 17.61% with symmetrically-shaped tensors for different  $k$ -order tensor layouts.

One can conclude that LOG-based tensor-times-matrix algorithms are on par or can even outperform TTGT-based and GETT-based implementations without losing their flexibility. Hence, other actively developed libraries such as LibTorch and Eigen might benefit from implementing the proposed algorithms. Our header-only library provides c++ interfaces and a python module which allows frameworks to easily integrate our library.

In the near future, we intend to incorporate our implementations in TensorLy, a widely-used framework for tensor computations [17, 18]. Currently, we lack a heuristic for selecting subtensor sizes and choosing the corresponding algorithm. Using the insights provided in [10] could help to further increase the performance. Additionally, we want to explore to what extent our approach can be applied for the general tensor contractions.

### 7.0.1. Source Code Availability

Project description and source code can be found at <https://github.com/bassoy/ttm>. The sequential tensor-matrix multiplication of TLIB is part of uBLAS and in the official release of Boost v1.70.0 and later.

## 955 References

- 956 [1] E. Karahan, P. A. Rojas-López, M. L. Bringas-Vega, P. A.  
957 Valdés-Hernández, P. A. Valdes-Sosa, Tensor analysis and fu-  
958 sion of multimodal brain images, *Proceedings of the IEEE*  
959 103 (9) (2015) 1531–1559.
- 960 [2] E. E. Papalexakis, C. Faloutsos, N. D. Sidiropoulos, Tensors for  
961 data mining and data fusion: Models, applications, and scal-  
962 able algorithms, *ACM Transactions on Intelligent Systems and*  
963 *Technology (TIST)* 8 (2) (2017) 16.
- 964 [3] N. Lee, A. Cichocki, Fundamental tensor operations for large-  
965 scale data analysis using tensor network formats, *Multidimen-*  
966 *sional Systems and Signal Processing* 29 (3) (2018) 921–960.
- 967 [4] T. G. Kolda, B. W. Bader, Tensor decompositions and applica-  
968 tions, *SIAM review* 51 (3) (2009) 455–500.
- 969 [5] B. W. Bader, T. G. Kolda, Algorithm 862: Matlab tensor classes  
970 for fast algorithm prototyping, *ACM Trans. Math. Softw.* 32  
971 (2006) 635–653.
- 972 [6] E. Solomonik, D. Matthews, J. Hammond, J. Demmel, Cyclops  
973 tensor framework: Reducing communication and eliminating  
974 load imbalance in massively parallel contractions, in: *Parallel &*  
975 *Distributed Processing (IPDPS)*, 2013 IEEE 27th International  
976 Symposium on, IEEE, 2013, pp. 813–824.
- 977 [7] P. Springer, P. Bientinesi, Design of a high-performance gemm-  
978 like tensor–tensor multiplication, *ACM Transactions on Math-*  
979 *ematical Software (TOMS)* 44 (3) (2018) 28.
- 980 [8] D. A. Matthews, High-performance tensor contraction without  
981 transposition, *SIAM Journal on Scientific Computing* 40 (1)  
982 (2018) C1–C24.
- 983 [9] E. D. Napoli, D. Fabregat-Traver, G. Quintana-Ortí, P. Bien-  
984 tinesi, Towards an efficient use of the blas library for multilin-  
985 ear tensor contractions, *Applied Mathematics and Computation*  
986 235 (2014) 454 – 468.
- 987 [10] J. Li, C. Battaglini, I. Perros, J. Sun, R. Vuduc, An input-  
988 adaptive and in-place approach to dense tensor-times-matrix  
989 multiply, in: *High Performance Computing, Networking, Stor-*  
990 *age and Analysis*, 2015, IEEE, 2015, pp. 1–12.
- 991 [11] Y. Shi, U. N. Niranjan, A. Anandkumar, C. Cecka, Tensor con-  
992 tractions with extended blas kernels on cpu and gpu, in: *2016*  
993 *IEEE 23rd International Conference on High Performance Com-*  
994 *puting (HiPC)*, 2016, pp. 193–202.
- 995 [12] C. Basso, Design of a high-performance tensor-vector multi-  
996 plication with blas, in: *International Conference on Computa-*  
997 *tional Science*, Springer, 2019, pp. 32–45.
- 998 [13] F. Pawłowski, B. Uçar, A.-J. Yzelman, A multi-dimensional  
999 morton-ordered block storage for mode-oblivious tensor com-  
1000 putations, *Journal of Computational Science* 33 (2019) 34–44.
- 1001 [14] A. Paszke, S. Gross, F. Massa, A. Lerer, J. Bradbury,  
1002 G. Chanan, T. Killeen, Z. Lin, N. Gimeshein, L. Antiga, et al.,  
1003 Pytorch: An imperative style, high-performance deep learning  
1004 library, *Advances in neural information processing systems* 32  
1005 (2019).
- 1006 [15] L.-H. Lim, Tensors and hypermatrices, in: L. Hogben (Ed.),  
1007 *Handbook of Linear Algebra*, 2nd Edition, Chapman and Hall,  
1008 2017.
- 1009 [16] C. Basso, V. Schatz, Fast higher-order functions for tensor cal-  
1010 culus with tensors and subtensors, in: *International Conference*  
1011 *on Computational Science*, Springer, 2018, pp. 639–652.
- 1012 [17] J. Cohen, C. Basso, L. Mitchell, Ttv in tensorly, *Tensor Com-*  
1013 *putations: Applications and Optimization* (2022) 11.
- 1014 [18] J. Kossaifi, Y. Panagakis, A. Anandkumar, M. Pantic, Ten-  
1015 sorly: Tensor learning in python, *Journal of Machine Learning*  
1016 *Research* 20 (26) (2019) 1–6.